Stress intensity factor analysis of friction sliding at discontinuity interfaces and junctions

A.-V. Phan[1], **L.J. Gray, T. Kaplan**

Computer Science and Mathematics Division, Oak Ridge National Laboratory, Oak Ridge, TN 37831-667, USA

J.A.L. Napier

CSIR, Division of Mining Technology, Auckland Park 2006, Johannesburg, SOUTH AFRICA

Abstract

Stress intensity factor (SIF) analysis in the context of fracture with frictional contact (crack friction) is presented. This analysis is carried out using our proposed framework for solving crack friction problems by the symmetric-Galerkin boundary element method (SGBEM), and the modified quarter-point (MQP) element developed in Ref. [11]. Since these problems are nonlinear, the proposed framework involves iterative calculations. As in case of non contact fracture, it is shown from this paper that, even incorporating the MQP element with a simple approach to compute SIFs such as the Displacement Correlation Technique (DCT), highly accurate SIFs can be obtained. With the MQP element, the mesh on the crack does not need to be excessively refined in order to achieve high accuracy for SIF results. This meshing advantage is especially more important in the context of frictional contact fracture, where the computing time of the iterative process strongly depends on the the number of elements used. Several numerical examples are presented and the SIF results are compared with available analytical solutions or references.

Keywords: stress intensity factor, crack friction, modified quarter-point element, boundary element method, symmetric-Galerkin approximation.

[1]Corresponding author: phana@ornl.gov

1 Introduction

The two principal approaches for computational fracture analysis are the finite element method (FEM) (e.g., [1]) and boundary element method (BEM) [2–5]. Note that displacement discontinuity method (DDM) proposed in [3] is a BEM fracture technique based on the analytical solution to the problem of a constant discontinuity in displacement over a single crack in an unbounded domain. The key feature of the integral equation approach is that only the boundary of the domain is discretized and only boundary quantities are determined. As a result, the singular stress field ahead of the crack is not approximated in the analysis, and moreover, remeshing a propagating crack is easier.

In both finite and boundary element modeling of discrete cracks, the standard approach consists of incorporating the stress singularity and critical $\sqrt{r}$ behavior at the crack tip, where r is the distance from a source point to the tip, by means of the 'quarter-point' (QP) element originally developed in References [6, 7]. Use of this QP element at the crack tip has significantly improved the accuracy of SIF calculations (*e.g.*, [8, 9]). Nevertheless, in either finite or boundary element analyses, the prediction of K_{II} and K_{III} has not been nearly as accurate as for K_I. Recently, Gray and Paulino [10] have proved that a constraint exists in the series expansion of the crack opening displacement about the tip. As discussed in [10], in general the QP element fails to satisfy this constraint, and this has led to the development of an improved element called modified QP [11]. It was also shown in [11] that the accuracy of the crack tip SIFs can be significantly improved by using the modified QP element. This would be important for crack propagation modeling.

Contact friction boundary conditions arise in problems relating to rolling and sliding between machine components or other bodies [12–14] and are ubiquitous in the fields of earthquake science, rock mechanics and geotechnical engineering, where multiple interacting faults and discontinuities are present. The numerical treatment of these problems often presents a number of difficulties in that boundary conditions are specified in the form of inequality constraints rather than in terms of fixed tractions or displacements. Further difficulties arise when multiple intersecting junctions are considered in a cracked material (kinked crack problems). For two-dimensional (2-D) problems, a rosette of interacting wedge structures have to be analyzed with, in general, power law displacement functions on each wedge face. Three-dimensional junctions are correspondingly more demanding. Thus far, FEM [15], BEM using an integral equation for the resultant forces along a crack [16–18], muti-domain BEM [19],dual BEM [20], and DDM [21–24] are numerical methods that have been employed for crack friction problems. Through the development of a framework for solving crack friction problems by the SGBEM, the goal of this work is to demonstrate that, by incorporating the modified QP element into the above SGBEM framework, even using a simple technique to compute SIFs such as the DCT, more accurate SIFs can be obtained with less iterative calculations for frictional contact fracture modeling including kinked crack problems.

This paper is organized as follows. In the next section, a review of the modified QP element is given. Section 3 briefly describes the SGBEM for fracture mechanics. In section 4, an algorithm using the SGBEM for solving crack friction problems is presented. In section 5, several numerical examples are solved and are compared with reference solutions. Finally, the last section contains some concluding remarks.

2. Modified Quarter-Point Element

2.1. Crack opening/sliding displacement expansion

For a crack geometry, the crack opening displacement (COD) Δu_k, $k = 1, 2$ in the neighborhood of the tip is [25, 26]

$$\Delta u_k(r,\theta) = b_k(\theta) r^{\frac{1}{2}} + c_k(\theta) r + d_k(\theta) r^{\frac{3}{2}} + \dots \ , \tag{1}$$

where r, θ are the distance to, and the direction emanating from, the tip, respectively.

It has been proved that, irrespective of the problem geometry or boundary conditions, the series expansion in Eq. (1) must have $c_k = 0$ for $\Delta \boldsymbol{u}$ *on the crack surface* [10] (for related work see Reference [27]), i.e.

$$\Delta u_k(r,\theta) = b_k(\theta) r^{\frac{1}{2}} + d_k(\theta) r^{\frac{3}{2}} + \dots \ . \tag{2}$$

It is known that the above equations have initially been established for crack opening. However, as shown through this paper, these relationships are also valid for crack closure cases. Thus, Eqs. 1 and 2 need to be intepreted as crack sliding displacement in case of crack closure problems.

2.2. Formulation of the modified quarter-point shape functions

The two-dimensional QP element is based upon the three-equidistant-noded quadratic element. For $t \in [0,\ 1]$, the shape functions for this element are given by

$$\begin{aligned} \psi_1(t) &= (1-t)(1-2t) \ , \\ \psi_2(t) &= 4t(1-t) \ , \\ \psi_3(t) &= t(2t-1) \ . \end{aligned} \tag{3}$$

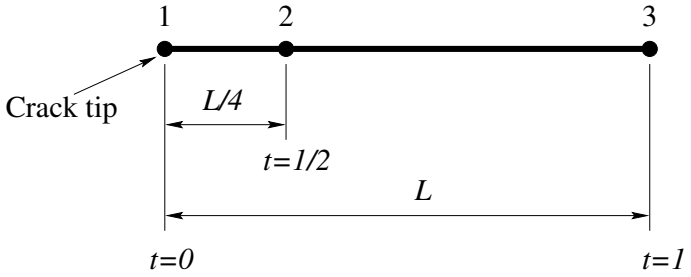

Figure 1: Crack tip element.

As $\Delta \boldsymbol{u} = 0$ at the crack tip, which is assumed to be at $t = 0$ (Fig. 1), the geometry and COD representations of the crack tip element are

$$\Gamma(t) = \sum_{j=1}^{3} (x_j \psi_j(t),\ y_j \psi_j(t)) \ , \tag{4}$$

$$\Delta u_k(t) = \sum_{j=2}^{3} \left(\Delta u_1^{(j)} \psi_j(t),\ \Delta u_2^{(j)} \psi_j(t) \right) \ , \tag{5}$$

where (x_j, y_j) are the coordinates of the three nodes defining the crack tip element, and $\Delta u_k^{(j)}$ the nodal values of the COD.

By moving the mid-node coordinates (x_2, y_2) three-fourths of the way towards the tip (see Fig. 1), the parameter t becomes $\sqrt{r/L}$, with L being the distance from (x_1, y_1) to (x_3, y_3) [6, 7]. As a consequence, the leading order term in $\Delta u_k^{(j)}$ at $t = 0$, which is t, is the correct square root of distance. Note however, that the next term, which is t^2, is r/L. According to Eq. (2), this term should vanish, and the modification presented in Reference [11] accomplishes the cancellation of this t^2 term. The resulting shape functions for the modified QP element is

$$\begin{aligned} \hat{\psi}_2(t) &= -\frac{8}{3}(t^3 - t) \,, \\ \hat{\psi}_3(t) &= \frac{1}{3}(4t^3 - t) \,, \end{aligned} \tag{6}$$

which should be used in Eq. (5) instead of $\psi_j(t)$. It can be observed that the modified shape functions (6) still satisfy the Kronecker delta property $\hat{\psi}_i(t_j) = \delta_{ij}$. This new approximation is only applied to the COD, as we keep the representation of $\Gamma(t)$ as in Eq. (4) so that the property $t \approx \sqrt{r}$ remains.

2.3. Stress Intensity Factors

SIFs provided by both the modified and standard QP elements will be calculated by means of the DCT. The point here is to assess the quality of the MQP in the context of frictional contact fracture by means a very simple method such as the DCT. The general expression of SIFs by means of the DCT technique are given by

$$\begin{aligned} K_I &= \frac{G}{\kappa + 1} \lim_{r \to 0} \sqrt{\frac{2\pi}{r}} \, \Delta u_2 \,, \\ K_{II} &= \frac{G}{\kappa + 1} \lim_{r \to 0} \sqrt{\frac{2\pi}{r}} \, \Delta u_1 \,, \end{aligned} \tag{7}$$

where $\boldsymbol{\Delta u}$ is the COD in the coordinate system associated with the crack tip under consideration, G is shear modulus, ν is Poisson's ratio, and

$$\kappa = 3 - 4\nu \quad \text{(plane strain)} \,, \qquad \kappa = \frac{3 - \nu}{1 + \nu} \quad \text{(plane stress)} \,. \tag{8}$$

For the standard QP element, it is known that by substituting Eqs. (3) and (5) in Eq. (7), one gets

$$\begin{aligned} K_I &= \frac{G}{\kappa + 1} \sqrt{\frac{2\pi}{L}} \, \left(4\Delta u_2^{(2)} - \Delta u_2^{(3)} \right) \,, \\ K_{II} &= \frac{G}{\kappa + 1} \sqrt{\frac{2\pi}{L}} \, \left(4\Delta u_1^{(2)} - \Delta u_1^{(3)} \right) \,. \end{aligned} \tag{9}$$

The SIFs in case of the modified QP element is obtained by a similar manner [11]. The result is

$$\begin{aligned} K_I &= \frac{G}{3(\kappa + 1)} \sqrt{\frac{2\pi}{L}} \, \left(8\Delta u_2^{(2)} - \Delta u_2^{(3)} \right) \,, \\ K_{II} &= \frac{G}{3(\kappa + 1)} \sqrt{\frac{2\pi}{L}} \, \left(8\Delta u_1^{(2)} - \Delta u_1^{(3)} \right) \,. \end{aligned} \tag{10}$$

Thus, SIFs are given directly in terms of the nodal values of the COD at the crack tip element.

3. Symmetric-Galerkin boundary integral formulation

This section provides a very brief review of boundary integral equations for elasticity, and their approximation via the symmetric-Galerkin procedure. The reader is asked to consult the cited references for further details.

The boundary integral equation (BIE) without body forces for linear elasticity is given by Rizzo [28]. For a source point P interior to the domain, this equation takes the form

$$u_k(P) - \int_{\Gamma_b} \left[U_{kj}(P,Q)\ \tau_j(Q) - T_{kj}(P,Q)\ u_j(Q) \right]\ dQ = 0\ , \tag{11}$$

where Q is a field point, τ_j and u_j are traction and displacement vectors, U_{kj} and T_{kj} are the Kelvin kernel tensors or fundamental solutions, Γ_b denotes the boundary of the domain, and dQ is an infinitesimal boundary length (for 2-D) or boundary surface (for 3-D cases).

It can be shown that the limit of the right hand side of Eq. (11) as P approaches the boundary exists. From now on, for $P \in \Gamma_b$, the BIE is understood in this limiting sense.

As P is off the boundary, the kernel functions are not singular and it is permissible to differentiate Eq. (11) with respect to P, yielding the hypersingular BIE (HBIE) for displacement gradient. Substitution of this gradient into Hooke's law gives the following HBIE for boundary stresses:

$$\sigma_{k\ell}(P) - \int_{\Gamma_b} \left[D_{kj\ell}(P,Q)\ \tau_j(Q) - S_{kj\ell}(P,Q)\ u_j(Q) \right]\ dQ = 0\ , \tag{12}$$

Expressions for the kernel tensors $U_{kj}, T_{kj}, D_{kj\ell}$ and $S_{kj\ell}$ can be found in, e.g., [29].

The Galerkin boundary integral formulation is obtained by taking the shape functions ψ_m employed in approximating the boundary tractions and displacements as weighting functions for the integral equations 11 and 12. Thus,

$$\int_{\Gamma_b} \psi_m(P)\ u_k(P)\ dP - \int_{\Gamma_b} \psi_m(P) \int_{\Gamma_b} \left[U_{kj}(P,Q)\ \tau_j(Q) - T_{kj}(P,Q)\ u_j(Q) \right] dQ\ dP = 0\ , \tag{13}$$

$$\int_{\Gamma_b} \psi_m(P)\ \sigma_{k\ell}(P)\ dP - \int_{\Gamma_b} \psi_m(P) \int_{\Gamma_b} \left[D_{kjl}(P,Q)\ \tau_j(Q) - S_{kjl}(P,Q)\ u_j(Q) \right] dQ\ dP = 0\ . \tag{14}$$

A symmetric coefficient matrix, and hence a symmetric-Galerkin approximation, is obtained by employing Eq. (13) on the boundary $\Gamma_{b(\boldsymbol{u})}$ where displacements u_{bv} are prescribed, and similarly using Eq. (14) is employed on the boundary $\Gamma_{b(\boldsymbol{\tau})}$ with prescribed tractions τ_{bv}. Note that $\Gamma_b = \Gamma_{b(\boldsymbol{u})} + \Gamma_{b(\boldsymbol{\tau})}$.

A solution procedure that employs a collocation approach enforces the BIE (11) and HBIE (12) at discrete source points whereas these equations are satisfied in an averaged sense with the Galerkin approximation. The additional boundary integration is the key to obtaining a symmetric coefficient matrix, as this ensures that the source point P and field point Q are treated in the same manner in evaluating the kernel tensors U_{kj}, T_{kj}, D_{kjl} and S_{kjl}. After discretization, the resulting equation system can be written as

$$\begin{bmatrix} H_{11} & H_{12} \\ H_{21} & H_{22} \end{bmatrix} \begin{Bmatrix} u_{bv} \\ u_* \end{Bmatrix} = \begin{bmatrix} G_{11} & G_{12} \\ G_{21} & G_{22} \end{bmatrix} \begin{Bmatrix} \tau_* \\ \tau_{bv} \end{Bmatrix}\ . \tag{15}$$

Here, the first and second rows represent, respectively, the BIE written on $(\Gamma_{b(\boldsymbol{u})})$ and the HBIE on $(\Gamma_{b(\boldsymbol{\tau})})$. Further, u_* and τ_* denote unknown displacement and traction vectors. Rearranging Eq. (15) into the form $[A]\{x\} = \{b\}$, and multiplying the HBIE by -1, one obtains

$$\begin{bmatrix} -G_{11} & H_{12} \\ G_{21} & -H_{22} \end{bmatrix} \begin{Bmatrix} \tau_* \\ u_* \end{Bmatrix} = \begin{Bmatrix} -H_{11}u_{bv} + G_{12}\tau_{bv} \\ H_{21}u_{bv} - G_{22}\tau_{bv} \end{Bmatrix}\ . \tag{16}$$

The symmetry of the coefficient matrix, $G_{11} = G_{11}^T$, $H_{22} = H_{22}^T$ and $H_{12} = G_{21}^T$ now follows from the symmetry properties of the kernel tensors.

3.1. Cracks in finite domains

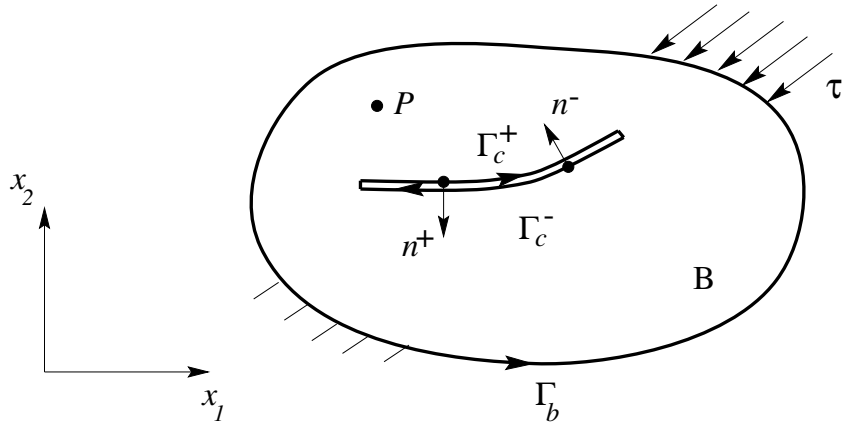

Figure 2: A body B containing a fracture.

A finite domain or body, B, of general shape is shown in Figure 2. The body is shown to include a crack surface denoted as Γ_c on which only tractions are prescribed. Initially, the crack is composed of two coincident surfaces according to $\Gamma_c = \Gamma_c^+ + \Gamma_c^-$ where Γ_c^+ and Γ_c^- denote the upper and lower crack surfaces, respectively. As a result, the outward normals to the crack surfaces, $\boldsymbol{n}_c^+$ and $\boldsymbol{n}_c^-$, are oriented oppositely so that $\boldsymbol{n}_c^- = -\boldsymbol{n}_c^+$. Thus, the BIE and HBIE written for an interior point P then take the following forms:

$$\begin{aligned} u_k(P) &= \int_{\Gamma_b} [U_{kj}(P,Q)\ \tau_j(Q) - T_{kj}(P,Q)\ u_j(Q)]\ dQ \\ &+ \int_{\Gamma_c^+} [U_{kj}(P,Q)\ \Sigma\tau_j(Q) - T_{kj}(P,Q)\ \Delta u_j(Q)]\ dQ\ , \end{aligned} \tag{17}$$

$$\begin{aligned} \sigma_{k\ell}(P) &= \int_{\Gamma_b} [D_{\ell km}(P,Q)\ \tau_m(Q) - S_{\ell km}(P,Q)\ u_m(Q)]\ dQ \\ &+ \int_{\Gamma_c^+} [D_{\ell km}(P,Q)\ \Sigma\tau_m(Q) - S_{\ell km}(P,Q)\ \Delta u_m(Q)]\ dQ\ , \end{aligned} \tag{18}$$

where, only the upper crack surface Γ_c^+ needs to be modeled as on the two crack surfaces, the displacements $\boldsymbol{u}_c^+$ and $\boldsymbol{u}_c^-$ are replaced by the single crack opening displacement (COD) $\Delta\boldsymbol{u}_c = \boldsymbol{u}_c^+ - \boldsymbol{u}_c^-$, and the tractions $\boldsymbol{\tau}_c^+$ and $\boldsymbol{\tau}_c^-$ by the sum of tractions $\Sigma\boldsymbol{\tau}_c = \boldsymbol{\tau}_c^+ + \boldsymbol{\tau}_c^-$. However, since the crack surfaces are usually symmetrically loaded, i.e $\boldsymbol{\tau}_c^- = -\boldsymbol{\tau}_c^+$, one gets

$$u_k(P) = \int_{\Gamma_b} [U_{kj}(P,Q)\ \tau_j(Q) - T_{kj}(P,Q)\ u_j(Q)]\ dQ - \int_{\Gamma_c^+} T_{kj}(P,Q)\ \Delta u_j(Q)\ dQ\ , \tag{19}$$

$$\sigma_{k\ell}(P) = \int_{\Gamma_b} [D_{\ell km}(P,Q)\ \tau_m(Q) - S_{\ell km}(P,Q)\ u_m(Q)]\ dQ - \int_{\Gamma_c^+} S_{\ell km}(P,Q)\ \Delta u_m(Q)\ dQ\ . \tag{20}$$

It can be shown that a symmetric coefficient matrix can be achieved by using $\Delta\boldsymbol{u}$ as variables on Γ_c^+. Following the Galerkin approximation, the limit of (19) and (20) is taken as $P \to \Gamma_{b(\boldsymbol{u})}$ and

$\Gamma_{b(\boldsymbol{\tau})}$, respectively. At this point, it is convenient to convert the stress equation (20) into a traction equation through the identity $\tau_k(P) = \sigma_{\ell k}(P)\, n_\ell(P)$, with $n_\ell(P)$ being the outward normal at P. After discretizing, the following system established from Eqs. (19) and (20) is obtained:

$$[G_{bb}]\,\{\tau_b\} = [H_{bb}]\,\{u_b\} + [H_{bc}]\,\{\Delta u_c\}\,, \tag{21}$$

where b and c denote the outer boundary and upper crack surface, respectively.

Since tractions are prescribed on the crack, only Eq. (20) is written for source points on Γ_c^+. Again, following the Galerkin approximation, the limit of (20) as $P \to \Gamma_c$, the conversion of (20) into a traction equation, and discretization, the result is

$$[G_{cb}]\,\{\tau_b\} - [G_{cc}]\,\{\tau_c^+\} = [H_{cb}]\,\{u_b\} + [H_{cc}]\,\{\Delta u_c\}\,. \tag{22}$$

Note that $\boldsymbol{\tau}_c^+$ now appears on the left hand side of Eq. (22) due to the limit process as $P \to \Gamma_c$. Combining Eqs. (21) and (22), the equation system of the problem can be written as follows:

$$\begin{bmatrix} H_{bb} & H_{bc} \\ H_{cb} & H_{cc} \end{bmatrix} \begin{Bmatrix} u_b \\ \Delta u_c \end{Bmatrix} = \begin{bmatrix} G_{bb} & 0 \\ G_{cb} & G_{cc} \end{bmatrix} \begin{Bmatrix} \tau_b \\ -\tau_c^+ \end{Bmatrix}, \tag{23}$$

where it can be proved that the coefficient matrix on the left hand side of (23) is also symmetric.

3.2. Cracks in unbounded domains

When an unbounded domain is considered and is subjected to uniform remote stress $\bar{\sigma}_{ij}$, Eq. (22) reduces to the following system:

$$-[G_{cc}]\,\{\tau_c^+\} = [H_{cc}]\,\{\Delta u_c\}\,, \tag{24}$$

where $\{\tau_c^+\}$ on the upper crack surface Γ_c^+ is now the superposition of the prescribed tractions directly applied on Γ_c^+ and the tractions $\bar{\sigma}_{ij}\, n_j^+$ due to the remote stresses $\bar{\sigma}_{ij}$. Note that n_j^+ are the components of the outward normal $\boldsymbol{n}_c^+$ to Γ_c^+.

4. Crack friction algorithm using the SGBEM

In this section, we present a framework to model cracks with frictional contact using the SGBEM. This is a nonlinear boundary value problem which can be resolved by adopting an iterative scheme. This scheme enables the determination of two important quantities, namely the normal tractions and crack sliding displacements (slip) on the sliding crack surfaces. Thus, mode-II SIF can be found by using the slip result in Eq. (10). In the following sections, it is shown that the symmetric-Galerkin procedure can also be formulated to resolve problems of friction sliding in cases where the friction constraint condition may be different on each branch of a common junction point.

4.1. Problem formulation

Consider a body B (or an unbounded domain) containing internal cracks subjected to prescribed global tractions $\boldsymbol{\tau}_c$. Let Δu_n and Δu_t be, respectively, the crack opening/closing and sliding displacements in the local coordinate system (t, n). After the final solution of the iterative scheme is converged, additional local tractions $\boldsymbol{t} = (t_t, t_n)$ on the sliding crack surfaces are determined such that no material interpenetration occurs. Note that t_n and t_t are, respectively, the normal and tangential components of $\boldsymbol{t}$. The boundary conditions for the final solution are

1. Either $\Delta u_n = 0$ and $\Delta u_t = 0$ (the crack is not sliding), in which case $\boldsymbol{t} = 0$, or
2. $\Delta u_n > 0$ (the crack is open), also in which case $\boldsymbol{t} = 0$, or
3. Δu_n is forced to be 0 (no material interpenetration, the crack is sliding) by applying additional tractions $\boldsymbol{t}$ on those crack surfaces; the normal and tangential components of $\boldsymbol{t}$ are related by $|t_t| = -\tan(\phi) t_n$ with ϕ being the friction angle. The sign of t_t is such that the sliding movement of the crack surfaces is opposed.

Note that t_n is nonlinearly dependent on the Δu_n values on all other cracks and on the field stress.

4.2. Iterative procedure

For crack friction problems, the numerical solution with the initial traction boundary conditions on the crack surfaces provides negative Δu_n (material interpenetration) in the region of contact. This negative Δu_n solution is obviously unphysical, and thus an iterative procedure is employed to determine t_n and t_t such that $\Delta u_n \geq 0$.

1. From the SGBEM solution for the global COD $\Delta \boldsymbol{u}_c$, compute the local displacement components Δu_n and Δu_t.
2. If $\Delta u_n < 0$ at a given node on the crack, set
   (a) Normal traction at the i^{th} step as $t_n^{(i)} = t_n^{(i-1)} - k\Delta u_n$, where $t_n^{(i-1)}$ is the normal traction at the previous step, and $k = G/b$ with G and b being the shear modulus and crack length, respectively,
   (b) $t_t = \text{sign}(\Delta u_t) \tan(\phi) t_n$.
3. At the crack tips of a sliding crack, normal tractions $t_n^{(i)}$ are determined by interpolating those at the other nodes of the crack tip elements.
4. Convert the local traction components t_n and t_t to the global traction vector $\boldsymbol{\tau}_{ca}^+$ on the upper crack surface.
5. Superpose the above additional tractions $\boldsymbol{\tau}_{ca}^+$ to the initially prescribed tractions $\boldsymbol{\tau}_c^+$ on the crack surface. Re-solve the SGBEM system (23).
6. Repeat from the first step until convergence.

The error indicator of convergence is calculated after each iterative step as the maximum difference between the current and previous computed local normal traction component

$$\epsilon = \max |t_n^{(i)} - t_n^{(i-1)}| \tag{25}$$

The iteration process is converged when the error indicator ϵ is below a specified tolerance ϵ_0.

5. Numerical examples

Four problems are reported in this section to illustrate the proposed algorithm using the SGBEM. Unless otherwise noted, the plane strain state is considered, the material constants employed are Young's modulus $E = 70000$ MPa and Poisson's ratio $\nu = 0.2$, and a convergence criterion $\epsilon_0 = 10^{-6}$ MPa is chosen.

5.1. Single crack under compression

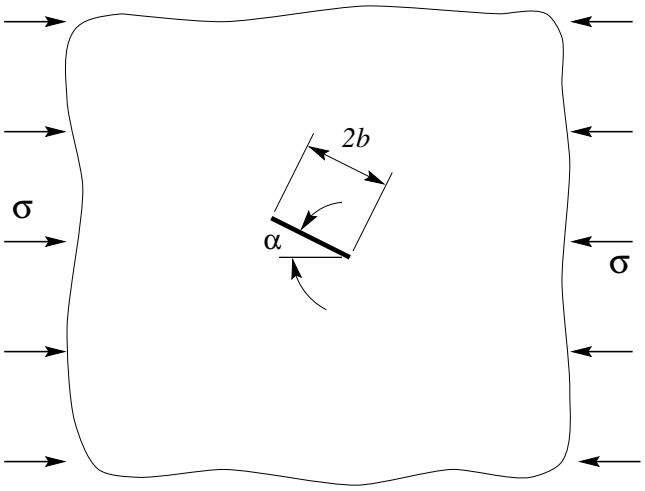

Figure 3: A crack under compression in an unbounded domain

A single crack of length $2b$ in an unbounded domain and subject to a compressive remote stress σ (see Fig. 3) is considered first, as an analytical solution is available for comparison. The following series of inclination angles $\alpha = 0^o, \ldots, 45^o$ and friction angles $\phi = 0^o, \ldots, 45^o$ are studied.

It is obvious that the mode-I SIF $K_I = 0$ as the crack surfaces remain closed under compression. The analytical solution for the mode-II SIF is given by [30]

$$K_{II} = \sigma \sqrt{\pi b} \sin\alpha(\cos\alpha - \tan\phi \sin\alpha) \, . \tag{26}$$

For numerical analysis by the SGBEM, the crack is discretized into ten quadratic elements of equal length. The numerical solution obtained with the MQP for $K_{II}/\sigma\sqrt{\pi b}$ (normalized K_{II}) is plotted in Fig. 4 together with the analytical solution. The solutions are almost identical. The performance of the MQP versus standard QP elements is compared in term of the ratio $K_{II}/K_{II}^{\text{exact}}$ listed in Table 1 for different inclination and friction angles α and ϕ. While the numerical result accuracy is consistent regardless the values of α and ϕ, the numerical solutions obtained with the MQP element are very accurate and much better than those obtained with the standard QP element. Note that the above remark remains valid for $\alpha = \phi = 45^o$. However, a comparison in term of $K_{II}/K_{II}^{\text{exact}}$ can not be shown as $K_{II}^{\text{exact}} = 0$ in this case.

Angle α	Crack tip element	Friction angle ϕ			
		0^o	15^o	30^o	45^o
15^o	QP	1.02334	1.02334	1.02335	1.02335
	MQP	0.99994	0.99994	0.99994	0.99994
30^o	QP	1.02334	1.02334	1.02334	1.02335
	MQP	0.99994	0.99994	0.99994	0.99994
45^o	QP	1.02334	1.02334	1.02335	N/A
	MQP	0.99994	0.99994	0.99994	N/A

Table 1: $K_{II}/K_{II}^{\text{exact}}$ as functions of inclination angle α and friction angle ϕ (10 crack elements)

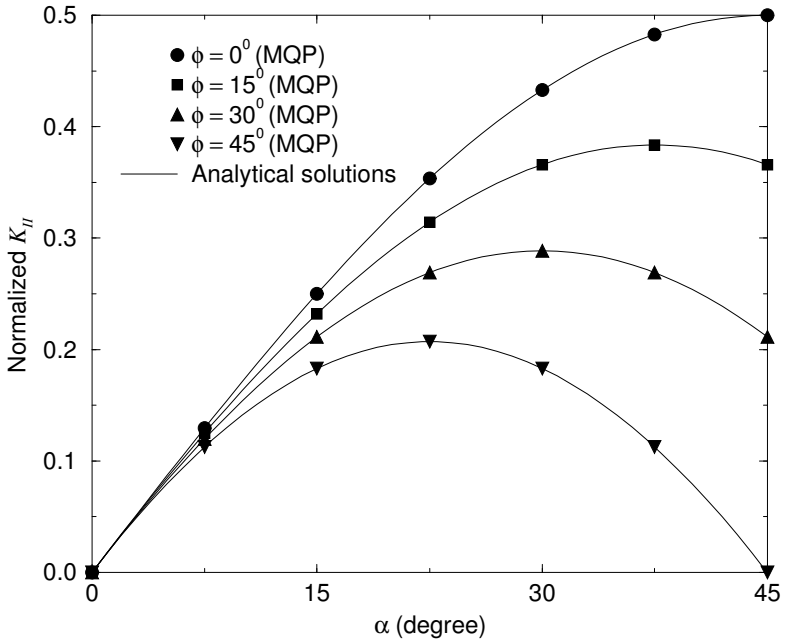

Figure 4: Numerical results vs. analytical solutions for normalized K_{II}

The primary advantage of the MQP over standard QP element in solving crack friction problems is illustrated by the comparison shown in Table 2. This table reveals that with the MQP element, the mesh on the crack does not need to be excessively refined as in case of standard QP element in order to obtain accurate SIF results. This advantage has also been observed in Ref. [11] in the context of non contact crack modeling. However, the achievement is much more significant in case of contact fracture which involves iterative calculations, as computing time is very expensive if excessively refined mesh is required. For the single crack under consideration, even a mesh of 100 elements with standard QP crack tip elements produces less accurate K_{II} result than that obtained from a mesh of only five crack elements with MQP crack tip elements. In addition, while the former case requires 2478 iterative steps, the latter only needs 178 steps. It is also interesting to note that with the same number of crack elements employed, the use of MQP element not only provides much more accurate solution, but also requires fewer iterative steps. This lower number of steps might be explained by the more accurate solutions for crack opening and crack sliding displacements near the crack tips provided by the MQP element during the iteration. Finally, as the number of crack elements is greater than ten, although the MQP solution accuracy decreases slightly, it appears that there is an asymptotic value for K_{II} which is still more accurate than the respective standard QP solution. This slightly decreasing accuracy may be explained by the fact that the crack tip element should be 'long enough' in order for the t^3 terms in the MQP shape functions (see Eq. (6)) to exhibit their presence [11].

The performance of using the SGBEM and MQP element in modeling crack friction problems can also be demonstrated by comparing our SIF results with those obtained from FROCK [24]. Consider a single closed crack in an infinite medium (see Fig. 3) with $2b = 0.0127$ m, $\alpha = 45^o$ and $\tan\phi = 0.364$. For numerical analysis, the crack is discretized into ten uniform quadratic elements. Figure 5 shows the mode-II SIF results obtained from the exact solution K_{II}^{exact} and from SGBEM

Number of crack elements	Crack tip element	$K_{II}/K_{II}^{\text{exact}}$	Number of iterative steps
5	QP	1.05015	186
	MQP	1.00144	178
10	QP	1.02335	329
	MQP	0.99994	319
20	QP	1.01097	607
	MQP	0.99961	585
30	QP	1.00698	866
	MQP	0.99956	836
40	QP	1.00500	1113
	MQP	0.99954	1079
50	QP	1.00383	1351
	MQP	0.99953	1313
75	QP	1.00227	1929
	MQP	0.99953	1871
100	QP	1.00149	2478
	MQP	0.99953	2403

Table 2: $K_{II}/K_{II}^{\text{exact}}$ and number of iterative steps as functions of number of crack elements ($\alpha = 20^o$ and $\phi = 30^o$)

using the MQP element K_{II} for different magnitudes of σ, while results for the ratio $K_{II}/K_{II}^{\text{exact}}$ are listed in Table 5. Again, these illustrations reveal that both solutions are almost identical. While our numerical solutions for K_{II} remain consistently accurate regardless any value of applied stress σ (see Tables 3), those obtained from FROCK and shown in Ref. [24] appear to be less accurate when the remote compressive stress σ exceeds 20 MPa.

Remote compressive stress σ (MPa)							
5	10	15	20	25	30	35	40
0.99994	0.99994	0.99994	0.99994	0.99994	0.99994	0.99994	0.99994

Table 3: $K_{II}/K_{II}^{\text{exact}}$ as a function of σ

5.2. Two-wing crack under compression

In this section, a two-wing crack in an unbounded domain and under uniaxial far-field compression as shown in Fig. 6 is investigated. This is the problem of kinked crack extension from an initially closed crack [31]. Due to the symmetry of this problem, SIFs at both crack tips are identical. The MQP element is employed to calculate these SIFs for different values of ratio c/b and kink angle θ, fixing orientation angle $\alpha = \pi/5$ and friction coefficient $\tan\phi = 0.3$. For numerical analysis by the SGBEM, non-uniform quadratic elements are used to discretize the initially closed crack and its two wings. This mesh refinement technique needs to be employed to treat the singularity in the dislocation densities at the crack kinks (junction points) [16].

The normalized SIF results ($K_I/\sigma\sqrt{\pi b}$ and $K_{II}/\sigma\sqrt{\pi b}$) are plotted in Figs. 7 and 8. It can

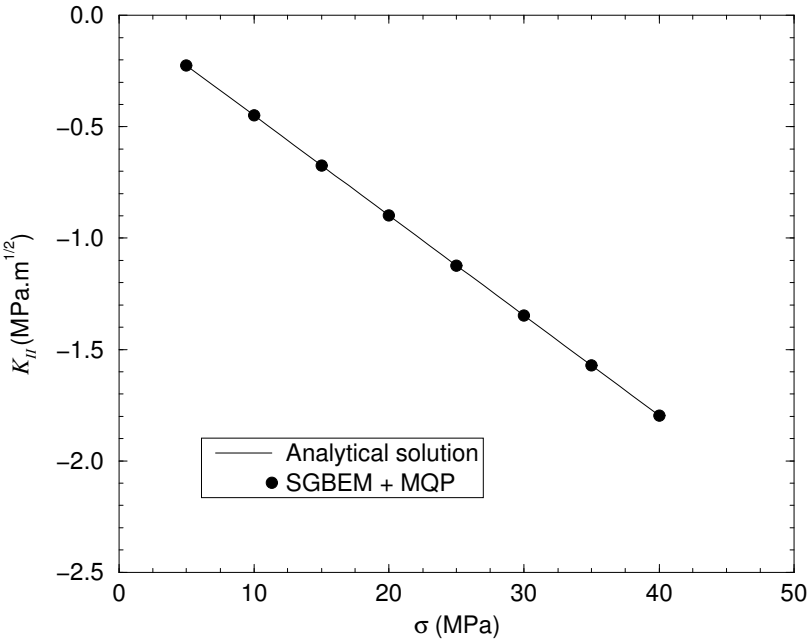

Figure 5: Numerical results vs. analytical solutions for K_{II}

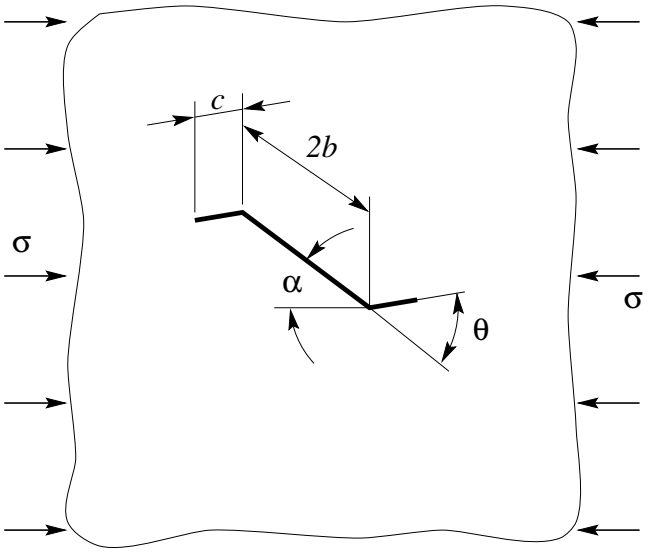

Figure 6: Two-wing crack in an unbounded domain

be observed that these results agree very well with those presented in Ref. [31] where a numerical method due to Gerasoulis [32] is used to solve a singular integral equation derived for the problem under consideration. It should be noted that, for a given value of c/b, θ, α and ϕ, the wings (crack kinking) remain closed when the angle θ is smaller than a certain value, and thus $K_I = 0$ in these cases (see Fig. 7). While our K_I solution properly interprets this closure situation, the numerical method employed in [31] provides $K_I < 0$ which represents material interpenetration.

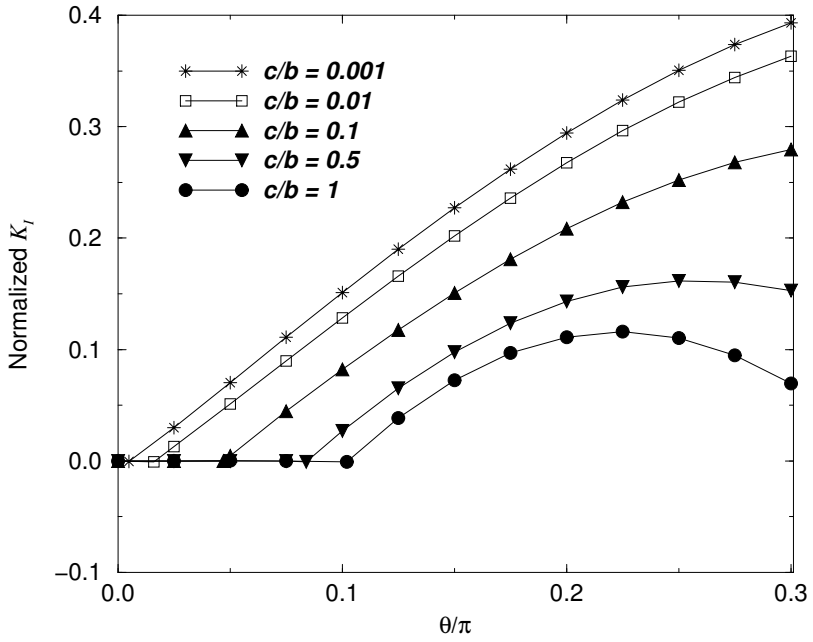

Figure 7: Normalized K_I solution ($\alpha = \pi/5$, $\tan\phi = 0.3$)

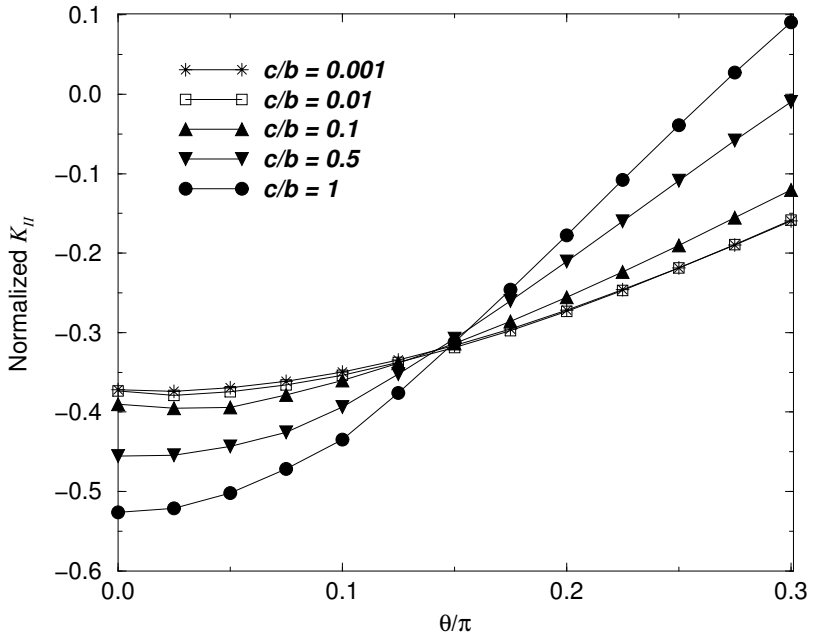

Figure 8: Normalized K_{II} solution ($\alpha = \pi/5$, $\tan\phi = 0.3$)

For the sake of reference, Tables 4 and 5 list the numeric values of normalized SIFs used to build the graphs shown in Figs. 7 and 8, respectively.

θ/π	c/b				
	0.001	0.01	0.1	0.5	1
0	-0.00009	-0.00009	-0.00009	-0.00010	-0.00009
0.025	0.02992	0.01298	-0.00009	-0.00009	-0.00009
0.05	0.07027	0.05102	0.00464	0.00001	0.00007
0.075	0.11101	0.08972	0.04444	-0.00008	-0.00009
0.1	0.15112	0.12830	0.08216	0.02684	-0.00097
0.125	0.18998	0.16600	0.11768	0.06528	0.03838
0.15	0.22710	0.20199	0.15089	0.09765	0.07241
0.175	0.26204	0.23608	0.18106	0.12356	0.09677
0.2	0.29446	0.26763	0.20843	0.14321	0.11110
0.225	0.32406	0.29638	0.23221	0.15596	0.11590
0.25	0.35054	0.32200	0.25211	0.16165	0.11035
0.275	0.37372	0.34431	0.26799	0.16063	0.09468
0.3	0.39344	0.36314	0.27964	0.15278	0.06967

Table 4: Numerical results for normalized K_I ($\alpha = \pi/5$, $\tan\phi = 0.3$)

θ/π	c/b				
	0.001	0.01	0.1	0.5	1
0	-0.37202	-0.37369	-0.38999	-0.45554	-0.52620
0.025	-0.37404	-0.37926	-0.39505	-0.45443	-0.52103
0.05	-0.36960	-0.37432	-0.39404	-0.44354	-0.50206
0.075	-0.36139	-0.36573	-0.37875	-0.42558	-0.47183
0.1	-0.34963	-0.35350	-0.36019	-0.39353	-0.43455
0.125	-0.33455	-0.33780	-0.33844	-0.35234	-0.37576
0.15	-0.31637	-0.31906	-0.31352	-0.30764	-0.31242
0.175	-0.29537	-0.29733	-0.28610	-0.26030	-0.24588
0.2	-0.27185	-0.27312	-0.25582	-0.21054	-0.17751
0.225	-0.24613	-0.24673	-0.22365	-0.15973	-0.10775
0.25	-0.21860	-0.21861	-0.19010	-0.10895	-0.03899
0.275	-0.18964	-0.18912	-0.15554	-0.05842	0.02723
0.3	-0.15964	-0.15865	-0.12066	-0.00952	0.09041

Table 5: Numerical results for normalized K_{II} ($\alpha = \pi/5$, $\tan\phi = 0.3$)

5.3. T-crack problem

Finally, consider a T-crack in an unbounded domain and subject to a remote compressive stress $\sigma = 100$ MPa acting vertically (see Fig. 9). The lengths of the vertical (opening) and horizontal (sliding) crack segments of this kinked crack are $c = 100$ m and $2b = 50$ m, respectively. The vertical

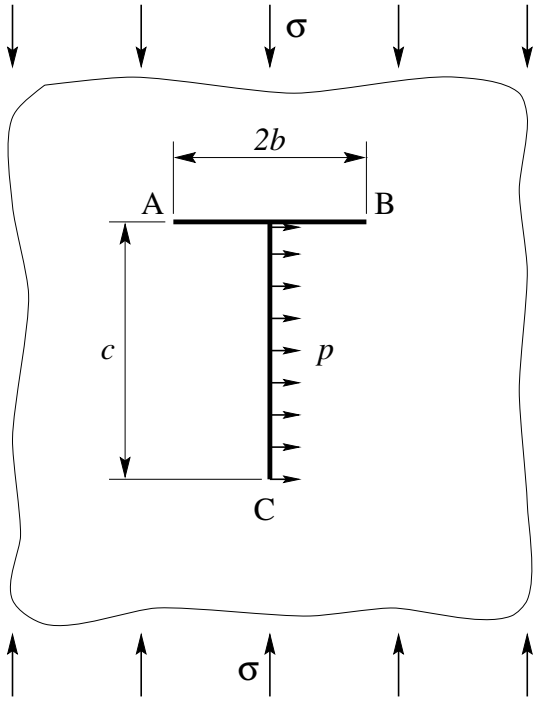

Figure 9: A T-crack in an unbounded domain

segment is horizontally pressurized to $p = 100$ MPa internally and intersects the the middle of the horizontal segment at right angles.

The SGBEM and MQP element are used to compute SIFs at the tips A, B, and C for frictional angle $\phi = 30^o$. The numerical results are compared with those obtained from the DDM using internal collocation [23]. For DDM simulation, 50/200 and 100/400 uniform elements (mesh 1/mesh 2) are employed to discretize the horizontal and vertical cracks, respectively. For SGBEM simulation, the corresponding number of elements are only 26 and 41. Again, since this is a kinked crack problem, mesh refinement technique needs to be used for the SGBEM analysis, with shorter elements being placed near the junction point. SIF results from both methods are listed in Table 6. Note that due to symmetry, at crack tips A and B, $K_{II\mathrm{A}} = -K_{II\mathrm{B}}$. Very good agreement from the numerical solutions can be observed. However, DDM needs to use an excessively refined mesh to obtain a result accuracy that only requires a coarse SGBEM mesh.

6. Conclusion

...

Acknowledgements

This research was supported in part by the Applied Mathematical Sciences Research Program of the Office of Mathematical, Information, and Computational Sciences, U.S. Department of Energy under contract DE-AC05-00OR22725 with UT-Battelle, LLC.

	$K_{I\mathrm{C}}/p\sqrt{\pi c}$	$K_{II\mathrm{A}}/\sigma\sqrt{\pi b}$
DDM (mesh 1)	0.7212	
DDM (mesh 2)	0.7169	
SGBEM	0.7166	

Table 6: SIFs at crack tips C and A

References

[1] Cook, R.D., Malkus, D.S., and Plesha, M.E., 1989, *Concepts and Applications of Finite Element Analysis*, John Wiley & Sons, New York.

[2] Cruse, T.A., 1988, *Boundary Element Analysis in Computational Fracture Mechanics*, Kluwer Academic Publishers, Boston.

[3] Crouch, S.L., and Starfield, A.M., 1990, *Boundary Element Methods in Solid Mechanics*, Unwin Hyman, London.

[4] Aliabadi, M.H., 1997, "Boundary Element Formulations in Fracture Mechanics," Applied Mechanics Reviews, **50**, pp. 83–96.

[5] Chen, J.T., and Hong, H.-K., 1999, "Review of dual boundary element methods with emphasis on hypersingular integrals and divergent series," Applied Mechanics Reviews, **52**, pp. 17–33.

[6] Henshell, R.D., and Shaw, K.G., 1975, "Crack tip finite elements are unnecessary," International Journal for Numerical Methods in Engineering, **9**, pp. 495–507.

[7] Barsoum, R.S., 1976, "On the use of isoparametric finite elements in linear fracture mechanics," International Journal for Numerical Methods in Engineering, **10**, pp. 25–37.

[8] Blandford, G.E., Ingraffea, A.R., and Liggett, J.A., 1981, "Two-dimensional stress intensity factor computations using the boundary element method," Int. J. Num. Meth. Engng, **17**, pp. 387–404.

[9] Banks-Sills, L., 1991, "Application of the finite element method to linear elastic fracture mechanics," Appl. Mech. Rev., **44**, pp. 447–461.

[10] Gray, L.J., and Paulino, G.H., 1998, "Crack tip interpolation, revisited," SIAM J. Applied Mathematics, **58**, pp. 428–455.

[11] Gray, L.J., Phan, A.-V., Paulino, G.H., and Kaplan, T., 2001, "Improved quarter-point crack tip element," Engineering Fracture Mechanics, (in press).

[12] Johnson, K.L., and Shercliff. H.R., 1992, "Shakedown of 2-dimensional asperities in sliding contact," International Journal of Mechanical Sciences, **34**, pp. 375–394.

[13] Man, K.W., Aliabadi, M.H., and Rooke, D.P., 1993, "BEM frictional contact analysis: load incremental technique," Computers & Structures, **47**, pp. 893–905.

[14] Huesmann, A., and Kuhn, G., 1995, "Automatic load incrementation technique for plane elastoplastic frictional contact problems using boundary element method," Computers & Structures, **56**, pp. 733–744.

[15] Ingraffea, A.R., and Heuze, F.E., 1980, "Finite element models for rock fracture mechanics," International Journal for Numerical and Analytical Methods in Geomechanics, **4**, pp. 25–43.

[16] Zang, W.L., and Gudmundson, P., 1990, "Contact problems of kinked cracks modelled by a boundary integral method," International Journal for Numerical Methods in Engineering, **29**, pp. 847–860.

[17] Zang, W.L., and Gudmundson, P., 1991, "Frictional contact problems of kinked cracks modelled by a boundary integral method," International Journal for Numerical Methods in Engineering, **31**, pp. 427–446.

[18] Chen, T.-C., and Chen, W.-H., 1998, "Frictional contact analysis of multiple cracks by incremental displacement and resultant traction boundary integral equations," Engineering Analysis with Boundary Elements, **21**, pp. 339–348.

[19] Liu, S.B., and Tan, C.L., 1992, "Two-dimensional boundary element contact mechanics analysis of angled crack problems," Engineering Fracture Mechanics, **42**, pp. 273–288.

[20] Lee, S.S., 1996, "Analysis of crack closure problem using the dual boundary element method," International Journal of Fracture, **77**, pp. 323–336.

[21] Chan, H.C.M., Li, V., and Einstein, H.H., 1990, "A hybridized displacement discontinuity and indirect boundary element method to model fracture propagation," International Journal of Fracture, **45**, pp. 263–282.

[22] Shen, B., and Stephansson, O., 1994, "Modification of the G-criterion for crack propagation subjected to compression," Engineering Fracture Mechanics, **47**, pp. 177–189.

[23] Napier, J.A.L., and Malan, D.F., 1997, "A viscoplastic discontinuum model of time-dependent fracture and seismicity in brittle rock," International Journal of Rock Mechanics and Mining Sciences, **34**, pp. 1075–1089.

[24] Bobet, A., and Einstein, H.H., 1998, "Numerical modeling of fracture coalescence in a model rock material," International Journal of Fracture, **92**, pp. 221–252.

[25] Williams, M.L., 1952, "Stress singularities resulting from various boundary conditions in angular corners of plates in extension," ASME J. Appl. Mech., **19**, pp. 526–528.

[26] Williams, M.L., 1957, "On the stress distribution at the base of a stationary crack," ASME J. Appl. Mech., **24**, pp. 109–114.

[27] Martin, P.A., 1991, "End-point behavior of solutions to hypersingular equations," Proc. R. Soc. Lond., A, **432**, pp. 301–320.

[28] Rizzo, F.J., 1967, "An integral equation approach to boundary value problems of classical elastostatics," Quarterly of Applied Mathematics, **25**, pp. 83–95.

[29] Bonnet, M., 1995, *Boundary Integral Equation Methods for Solids and Fluids*, John Wiley & Sons, England.

[30] Melville, P.H., 1977, "Fracture Mechanics of brittle materials in compression," International Journal of Fracture, **13**, pp. 532–534.

[31] Nemat-Nasser, S., and Horii, H., 1982, "Compression-induced nonplanar crack extension with application to spitting, exfoliation, and rockbust," Journal of Geophysical Research, **87**, pp. 6805–6821.

[32] Gerasoulis, A., 1982, "The use of piecewise quadratic polynomials for the solution of singular integral equations of Cauchy type," Computers & Mathematics with Applications, **8**, pp. 15–xx.